Inorg. Chem. **2005**, *44*, 9938–9945

Synthesis of WO_3 Nanorods by Reacting $WO(OMe)_4$ under Autogenic Pressure at Elevated Temperature Followed by Annealing

S. V. Pol,[†] V. G. Pol,[†] V. G. Kessler,[‡] G. A. Seisenbaeva,[‡] L. A. Solovyov,[§] and A. Gedanken*[,†]

Department of Chemistry and Kanbar Laboratory for Nanomaterials at the Bar-Ilan University Center for Advanced Materials and Nanotechnology, Bar-Ilan University, Ramat-Gan 52900, Israel, Department of Chemistry, SLU, Box 7015, 75007 Uppsala, Sweden, and Institute of Chemistry and Chemical Technology, K. Marx Av. 42, Krasnoyarsk 660049, Russia

Received July 14, 2005

This article reports on the fabrication of WO_3 nanorods using an efficient straightforward synthetic technique, without a catalyst, and using a single precursor. The thermal dissociation of $WO(OMe)_4$ at 700 °C in a closed Swagelok cell under an air/inert atmosphere yielded $W_{18}O_{49}$ nanorods. Annealing of $W_{18}O_{49}$ at 500 °C under an air atmosphere led to the formation of pure WO_3 nanorods. The obtained products are characterized by morphological (scanning electron microscopy and transmission electron microscopy), structural (X-ray diffraction analysis, high-resolution scanning electron microscopy, and Raman spectroscopy), and compositional [energy-dispersive X-ray and elemental (C, H, N, S) analysis] measurements. The mechanism of the formation of nonstoichiometric $W_{18}O_{49}$ nanorods is supported by the measured analytical data and several control experiments.

Introduction

Tungsten trioxide (WO_3) has been the subject of great interest as a result of its special electrochromic,[1,2] gas sensing,[3,4] and catalytic properties.[5] For these applications the morphological characteristics of the materials, such as grain size or shape, are very important and depend strongly on the preparation method. Nanopowders of WO_3 have been prepared by sol−gel,[6] spray pyrolysis,[7] and radio frequency magnetron sputtering.[8] It is well-known that certain significant properties of the materials are not governed only by the structure of the material itself but by faults or defects in the materials. WO_{3-x} showed sheet superconductivity, which is closely related to its substructures and defects.[9] A variety of methods have been developed to prepare tungsten oxide nanotubes[10] and nanorods or nanowires.[11] In most cases, the tungsten oxide products are a mixture of WO_3 and its suboxides with complex crystallographic defects. An interesting micrometer-scale product is a treelike structure of tungsten oxide that has been generated by heating a W foil that is partly covered by a SiO_2 plate under an Ar atmosphere at about 1600 °C.[12] The improvement in the electrochromic coloration efficiency (10-fold) by oxygen deficiency in sputtering WO_x films was described by an intervalence charge-transfer transition mechanism between localized W^{5+} and W^{6+} states.[13] An inorganic route for the controlled synthesis of $W_{18}O_{49}$ nanorods and nanofibers was developed by Lou et al., and the important role of a Na_2SO_4 salt in the synthesis has been demonstrated.[14] However, a high temperature and a complicated control process were required for such approaches.

* To whom correspondence should be addressed. E-mail: gedanken@mail.biu.ac.il. Phone: +972-353-18315. Fax: +972-3-535125.
† Bar-Ilan University.
‡ SLU.
§ Institute of Chemistry and Chemical Technology.

(1) Bange, K.; Gambke, T. *Adv. Mater.* **1990**, *2*, 10.
(2) Yih, S. W. H.; Wang, C. T. *Tungsten: Sources, Metallurgy, Properties and Applications*; Plenum Press: New York, 1979.
(3) Wang, Y. D.; Chen, Z. X.; Li, Y. F.; Zhou, Z. L.; Wu, X. H. *Solid-State Electron.* **2001**, *45*, 639.
(4) Antonik, M. D.; Schneider, J. E.; Wittman, E. L.; Snow, K.; Vetelino, J. F. *Thin Solid Films* **1995**, *256*, 247.
(5) Hattori, H.; Asada, N.; Tanabe, K. *Bull. Chem. Soc. Jpn.* **1978**, *51*, 1704.
(6) Badilescu, S.; Ashrit, P. V. *Solid State Ionics* **2003**, *158*, 187.
(7) Regragui, M.; Addou, M.; Outzourhit, A.; Bernede, J. C.; Idrissi, E. E.; Benseddik, E.; Kachouane, A. *Thin Solid Films* **2000**, *358*, 40.
(8) LeGore, L. J.; Lad, R. J.; Moulzolf, S. C.; Vetelino, J. V.; Frederik, B. G.; Kenik, E. A. *Thin Solid Films* **2002**, *406*, 79.
(9) Aird, A.; Salje, E. K. H. *J. Phys.: Condens. Matter* **1998**, *10*, 377.
(10) Li, Y. B.; Bando, Y.; Golberg, D. *Adv. Mater.* **2003**, *15*, 1294.
(11) Gu, G.; Zheng, B.; Han, W. Q.; Roth, S.; Liu, J. *Nano Lett.* **2002**, *2*, 849.
(12) Zhu, Y. Q.; Hu, W. B.; Hsu, W. K.; Terrone, M.; Grobert, N.; Hare, J. P.; Kroto, H. W.; Walton, D. R. M.; Terrones, H. *Chem. Phys. Lett.* **1999**, *309*, 327.
(13) Ho, J. J.; Chen, C. Y.; Lee, W. J. *Electron. Lett.* **2004**, *40*, 510.
(14) Lou, X. W.; Zeng, H. C. *Inorg. Chem.* **2003**, *42*, 6171.

10.1021/ic051179n CCC: $30.25 © 2005 American Chemical Society
Published on Web 11/17/2005

Table 1. Summary of the Reactant(s), the Reaction Conditions (Temperature, Time, and Atmosphere inside the Reaction Cell), the Obtained Morphology, and the Achieved Products

expt no.	reactant	temp/time/atmosphere	TEM morphology	product
1	$WO(OMe)_4$	700 °C/3 h/nitrogen	$W_{18}O_{49}$ + carbon	$W_{18}O_{49}$ + C
2	$WO(OMe)_4$	700 °C/3 h/air	WO_x + carbon	$W_{18}O_{49}$ + C
3	$W[OCH(CH_3)_2]_6$, 5% (w/v) in 2-propanol	700 °C/3 h/nitrogen	core (WO_x)−shell (carbon)	$W_{24}O_{68}$ + C
4	$WO(OMe)_4$, ethanol	700 °C/3 h/nitrogen	core (WO_x)−shell (carbon)	WO_2 + $W_{18}O_{49}$ + C
5	$WO(OMe)_4$, ice[a]	700 °C/3 h/nitrogen	no core−shell	WO_3

[a] The 20% (w/w) aqueous solution of $WO(OMe)_4$ was frozen to form ice, and then the formed precursor was used to carry out the RAPET at 700 °C for 3 h.

The one-stage, catalyst-free, efficient, and simplest synthetic technique for the fabrication of $W_{18}O_{49}$ nanorods using a single precursor was accounted for in this article. The thermal decomposition of $WO(OMe)_4$ at 700 °C in a closed Swagelok cell under an inert atmosphere yielded $W_{18}O_{49}$. Following this step with annealing the product at 500 °C under air led to the formation of pure WO_3 nanorods. Similar reactions were recently carried out in our research group for various organic or inorganic precursors, and the reactions were termed RAPET (reactions under autogenic pressure at elevated temperature). High-surface-area nano-SiC,[15] metastable phases of Co and ZrO_2 nanoparticles,[16] Si coated on spherical carbon,[17] uniform 2.5 ± 0.05 μm carbon spherules,[18] core−shell nanostructures of metals/metal oxides with carbon,[19] encapsulation of superconducting $MgCNi_3$ in a carbon nanoflask,[20] and fullerene-like[21] Ni−C are the interesting nanoproducts prepared using a similar RAPET method. The effects of an applied magnetic field on the RAPET of $MoO(OMe)_4$,[22] mesitylene,[23] and $CoZr_2(acac)_2$-$(O^iPr)_8$[24] are also reported.

2. Experimental Section

2.1. Synthesis and Gas-Phase Behavior of Precursor Compounds. The synthesis of the $WO(OMe)_4$ precursor has been carried out, as described elsewhere,[25,26] by the anodic oxidation of tungsten metal in refluxing methanol with lithium chloride as the electrolyte, at a total voltage of 50 V, and at a constant current of 150 mA. The initial crude product was recrystallized from hexane. Tungsten oxomethoxide, applied here as the precursor, is highly volatile at reduced pressure. Its evaporation led to the almost complete dissociation of the dimeric $[WO(OMe)_4]_2$ molecules present in the solid. The major route of transformation, according to the mass spectra, was just a symmetric cleavage of the molecule into two $WO(OMe)_4$ fragments, while a minor one was associated with the asymmetric cleavage occurring through the transfer of an oxoligand and the release of the new species, $W(OMe)_6$ and $WO_2(OMe)_2$. The ether elimination and β-hydrogen atom transfer played only very small roles in the side reactions on the evaporation of $WO(OMe)_4$, in contrast to that of $MoO(OMe)_4$.[27]

2.2. Fabrication of $W_{18}O_{49}$ Nanorods and Their Conversion to WO_3 Nanorods. The fabrication of $W_{18}O_{49}$ nanorods was carried out by introducing the $WO(OMe)_4$ precursor into a 2-mL closed cell. The cell was assembled from stainless steel Swagelok parts. A 1/2-in. union part was capped on both sides by standard plugs. For these syntheses, 0.5 g of the above precursor was introduced into the cell at room temperature under nitrogen (a nitrogen-filled glovebox). The filled cell was closed tightly by the other plug and then placed inside an iron pipe in the middle of the furnace. The temperature was raised at a heating rate of 10 °C/min. The closed-vessel cell was heated at 700 °C for 3 h. The reaction took place under the autogenic pressure of the precursor. The Swagelok was gradually cooled (~5 h) to room temperature and opened, and a black powder was obtained. The total yield of the product material was 89.6% of the total weight of the materials introduced in the cell. [The yield was the final weight of the product relative to the weight of $WO(OMe)_4$, the starting material.] The synthesis of nanomaterials by the RAPET method required the use of simple equipment, a comparatively low temperature, and a short reaction time to create one-dimensional pure $W_{18}O_{49}$ nanorods. The as-prepared WO_{3-x} nanorods were further annealed at 500 °C under an air atmosphere. The annealing led to the formation of pure yellow-colored WO_3 nanorods. The additional control experiments, reactant(s) used, reaction conditions (temperature, time, and atmosphere inside the reaction cell), obtained morphology, and reaction products are summarized in Table 1.

2.3. Characterizations. The X-ray diffraction (XRD) pattern of the products was measured with a Bruker AXS D* Advance powder X-ray diffractometer (using Cu Kα = 1.5418 radiation). Elemental analysis of the $W_{18}O_{49}$ and WO_3 samples was carried out on an Eager 200 C, H, N, S analyzer. The elemental composition of the materials and the scanning electron microscopy (SEM) images were analyzed by energy-dispersive X-ray (EDX) analysis on a JEOL-JSM 840 scanning electron microscope. The particle morphology and structure were studied with transmission electron microscopy (TEM) on a JEOL-JEM 100 SX microscope, working at an 80-kV accelerating voltage and with a JEOL-2010 high-resolution transmission electron microscopy (HRTEM) instrument, using an accelerating voltage of 200 kV. Samples for TEM and HRTEM were prepared by ultrasonically dispersing the $W_{18}O_{49}$ or WO_3 products into absolute ethanol, placing a drop of this suspension onto a copper grid coated with an amorphous carbon film, and then

(15) Pol, V. G.; Pol, S. V.; Gedanken, A. *Chem. Mater.* **2005**, *17*, 1797.
(16) Pol, S. V.; Pol, V. G.; Seisenbaeva, G.; Kessler, V. G.; Gedanken, A. *Chem. Mater.* **2004**, *16*, 1793.
(17) Pol, V. G.; Pol, S. V.; Gedanken, A.; Goffer, Y. *J. Mater. Chem.* **2004**, *14*, 966.
(18) Pol, V. G.; Motie, M.; Calderon-Moreno, J.; Yoshimura, M.; Gedanken, A. *Carbon* **2004**, *42*, 111.
(19) Pol, S. V.; Pol, V. G.; Gedanken, A. *Chem.−Eur. J.* **2004**, *10*, 4467.
(20) Rana, R. K.; Pol, V. G.; Felner, I.; Meridor, E.; Frydman, A.; Gedanken, A. *Adv. Mater.* **2004**, *16*, 972.
(21) Pol, S. V.; Pol, V. G.; Frydman, A.; Churilov, G. N.; Gedanken, A. *J. Phys. Chem. B* **2005**, *109*, 9495−98.
(22) Pol, S. V.; Pol, V. G.; Kessler, V. G.; Seisenbaeva, G. A.; Sung, M.; Asai, S.; Gedanken, A. *J. Phys. Chem. B* **2004**, *108*, 6322−27.
(23) Pol, V. G.; Pol, S. V.; Gedanken, A.; Sung, M.-G.; Shigeo, A. *Carbon* **2004**, *42* (12−13), 2738−41.
(24) Pol, V. G.; Pol, S. V.; Gedanken, A. *J. Phys. Chem. B* **2005**, *109*, 6121.
(25) Seisenbaeva, G. A.; Werndrup, P.; Kloo, L.; Kessler, V. G. *Inorg. Chem.* **2001**, *40*, 3815.
(26) Kessler, V. G.; Panov, A. N.; Turova, N. Y.; Starikova, Z. A.; Yanovsky, A. I.; Dolgushin, F. M.; Pisarevsky, A. P.; Struchkov, Y. T. *J. Chem. Soc., Dalton Trans.* **1998**, 21.
(27) Kozlova, N. I.; Kessler, V. G.; Turova, N. Y.; Belokon, A. I. *Koord. Khim.* **1989**, *15*, 1524.

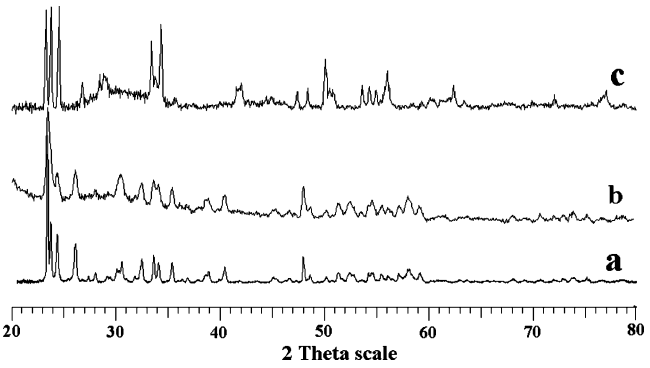

Figure 1. PXRD pattern of (a) the thermally decomposed $WO(OMe)_4$ at 700 °C under an inert atmosphere, (b) the thermally decomposed $WO(OMe)_4$ at 700 °C under an air atmosphere, and (c) the thermally decomposed $WO(OMe)_4$ at 700 °C under an air atmosphere and further annealed at 500 °C under an air atmosphere.

drying under air. The Olympus BX41 (Jobin−Yvon−Horiba) Raman spectrometer was employed, using the 514.5-nm line of an Ar ion laser as the excitation source to analyze the nature of the nanorods. A Micromeritics (Gemini 2375) surface area analyzer was used to measure the surface area of the $W_{18}O_{49}$ and WO_3 samples.

3. Results and Discussion

3.1. Powder X-ray Diffraction (PXRD), SEM, EDX Analysis, and Elemental (C, H, N, S) Analysis. The XRD patterns of the thermally decomposed $WO(OMe)_4$ at 700 °C in a closed Swagelok cell under an inert atmosphere are presented in Figure 1. In Figure 1a, a representative XRD pattern for our as-synthesized tungsten oxide nanorods is displayed (Table 1, expt no. 1). All the main peaks can be indexed undisputedly to monoclinic $W_{18}O_{49}$ [powder diffraction file (PDF) no. 36-101]. The ratio of the intensity of the ⟨010⟩ diffraction peak at $2\Theta = 23.5°$ to the intensity of the other diffraction peaks of the $W_{18}O_{49}$ nanorods was much larger than this ratio in the standard PDF table, indicating that ⟨010⟩ is the major growth direction.[15] It was expected that changing the atmosphere inside the reaction cell to an air atmosphere would lead to the formation of WO_3 nanorods. However, this control experiment also led to the formation of substoichiometric $W_{18}O_{49}$ (Figure 1b). The XRD of these products, obtained under an air atmosphere, showed pronounced diffraction peak broadening (Table 1, expt no. 2) as compared to the diffraction peaks of the sample prepared under an inert nitrogen atmosphere. Assuming that the width of the diffraction is only due to the size of the particle and not a result of microstrains and lattice defects would imply that the decomposition of $WO(OMe)_4$, under an air atmosphere, favors the formation of $W_{18}O_{49}$ rods having a smaller size.

Because the $WO(OMe)_4$ decomposition was carried out in a closed Swagelok cell, it was anticipated to have impurities such as carbon and hydrogen in addition to $W_{18}O_{49}$. The content of carbon and hydrogen in the product/carbonaceous material was examined by an elemental analysis measurement. We have calculated the element (wt) percent of carbon and hydrogen in the precursor solution and compared it with the elemental analysis data of the product. The calculated element percent of carbon in the precursor solution was 14.8% (in 0.5 g of precursor), while the percentage of hydrogen was 3.7%. The measured element percentage of carbon in the as-prepared product was 10.3% (in 0.448 g of product), while the percentage of hydrogen is 0.2%, and the rest of the product was $W_{18}O_{49}$. EDX analysis gave an O/W atomic ratio of 2.6 ± 0.3, which was in good agreement with the theoretical value of $W_{18}O_{49}$. Considering the presence of W_xO_y and carbon, the formed product was termed a "tungsten oxide−carbon" (TOC) composite (Table 1, expt no. 1). To get rid of the carbon, the TOC composite was annealed at 500 °C under an air atmosphere. The elemental (C, H, N, S) analysis detected 0% carbon and 0% hydrogen in the product after the annealing process. Furthermore, the TOC composite was turned into a pure WO_3 compound, evidenced by the XRD pattern shown in Figure 1c. The diffraction peaks, peak intensities, and cell parameters were in agreement with the diffraction peaks of the crystalline monoclinic phase of WO_3 (PDF no. 1-75-2072). The peaks of monoclinic WO_3 are narrower compared to those of $W_{18}O_{49}$, indicating either a crystallite growth or the release of a microstrain during the annealing.

The anisotropic morphologies of the products were observed by SEM and TEM analysis. The morphology of the TOC composite and the WO_3 obtained after annealing at 500 °C under an air atmosphere was primarily investigated by SEM measurements. The sample had a morphology composed of elongated (∼95%) and spherical particles (∼5%; Figure 2a). The elongated particles (rods) had an average diameter of ∼200 nm and a length of a few micrometers. The rods were polydispersed in nature. A few spherical bodies (indicated by an arrow) having a diameter of around 2.5 μm were identified by EDX as carbon spherules. The distinction between the elongated and the spherical bodies was made by using selected area energy dispersive X-ray (SAEDX) analysis attached to the SEM instrument. EDX measurements of the TOC composite revealed the presence of W, O, and C (Figure 2b). On the other hand, for the spherical particles, only the presence of C was detected (inset in Figure 2b). The carbon peak was more intense for the spherical carbon than the peak measured for the bare carbon-coated copper support. The carbon bodies completely disappeared after the annealing treatment. The stacking of two or more nanorods (indicated by arrows) could be observed. This rod assembly might be due to the rods sintering at 500 °C under an air atmosphere. The diameters of these rods increased up to 500 nm (Figure 2c and the XRD pattern shown in Figure 1c).

3.2. TEM and HRTEM Measurements. The structure of the TOC composite was further studied by TEM and HRTEM measurements. The TEM image (Figure 3a) demonstrated the rod-shaped morphology of the TOC composite after the thermal decomposition of $WO(OMe)_4$ at 700 °C. The as-formed $W_{18}O_{49}$ nanorods had average diameters in the range of 80−700 nm and lengths of several micrometers. The aspect ratio of the formed $W_{18}O_{49}$ nanorods varied drastically. An inset in Figure 3a shows an individual nanorod possessing a smooth surface with a diameter of 80

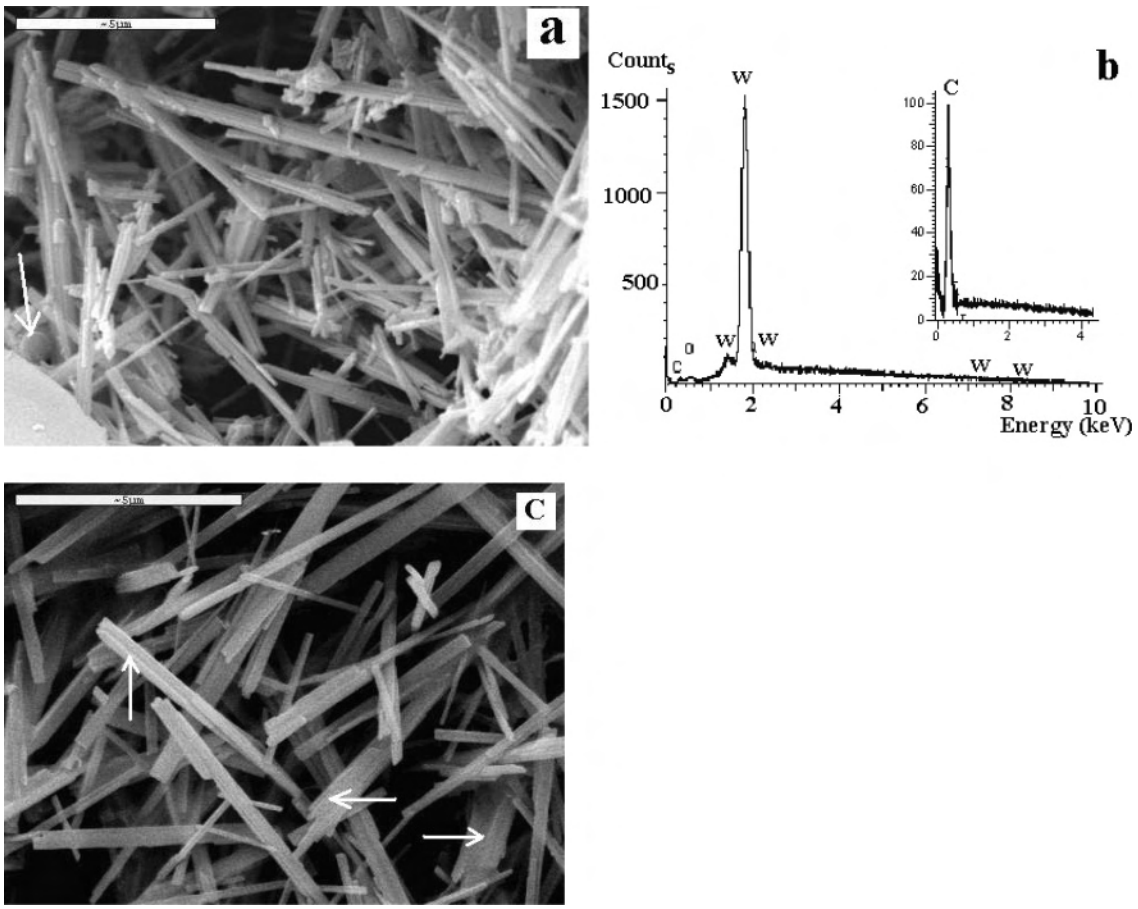

Figure 2. SEM images of (a) a TOC composite, (b) an EDX analysis of a tungsten oxide rod (inset: EDX of carbon spherules, indicated by an arrow), and (c) a TOC composite annealed at 500 °C under an air atmosphere.

nm and a length of 1.5 μm. Figure 3b presents an HRTEM image of a single $W_{18}O_{49}$ nanorod at the edge. The lattice spacing along $\langle 010 \rangle$ was determined as $d_{010} = 0.38 \pm 0.01$ nm, which is in excellent agreement with the reported lattice constant of monoclinic $W_{18}O_{49}$.[14] The corresponding electron diffraction (ED) pattern was demonstrated in Figure 3c, featuring a single crystal of monoclinic $W_{18}O_{49}$ particles (respective planes are highlighted). The presence of streaking lines in the ED pattern revealed that numerous stacking faults had formed in the direction normal to the $\langle 010 \rangle$ direction.[10]

The shape of the as-prepared material was unchanged upon heating in oxygen, implying that the nanorods were not damaged, destroyed, or deformed during annealing at 500 °C. The stacking or gathering of nanorods was the major change observed after the sintering process (Figure 3d). The lattice spacing of 0.365 nm was equal to the *d* value of $\langle 200 \rangle$ planes for monoclinic WO_3 (Figure 3e). The ED pattern shown in Figure 3f was obtained from the nanorod shown in the inset. The diffraction pattern indicated the single-crystal structure of WO_3 with a high degree of crystallinity.

The results of the Brunauer−Emmett−Teller surface area measurements of the as-prepared TOC composite prepared under an inert atmosphere, the TOC composite prepared under an air atmosphere, and the TOC composite sintered at 500 °C under air [tungsten oxide nanorods (TONR)] are 86.3, 66.6, and 2.5 m^2/g, respectively. The drastic reduction of the surface area of TONR might be due to the loss of the porous carbon on one hand and the sintering of a few WO_3 rods on the other hand. In addition to the elemental (C, H, N, S) analysis, the presence and nature of carbon in the TOC composite were studied by Raman spectroscopy measurements. The micro-Raman spectra of the TOC and WO_3 nanorods were measured and are presented in Figure 4. The major Raman bands of tungsten oxide (Figure 4a) were detected at 260, 326, 700, and 800 cm^{-1} for the TOC ($W_{18}O_{49}$−C) sample, while the Raman bands of pure WO_3 nanorods were measured at 271, 326, 700, and 800 cm^{-1} (Figure 4b). These bands fell exactly at wavenumbers of the fundamental modes of monoclinic WO_3 films.[28,29] The band at 271 cm^{-1}, assigned to the stretching O−W−O vibration of the bridging oxygen, shifted to 260 cm^{-1} for the TOC sample. The additional small Raman bands that appeared only in the TOC spectrum confirmed the presence of carbon (Figure 4a). The two characteristic bands of carbon[30] were detected at 1341 cm^{-1} (D band) and at 1597 cm^{-1} (G band). The intensity of the G band, associated with graphitic carbon, was larger for the TOC sample than the intensity of the D band. The intensity ratio of the D and G bands was $I_D/I_G = 0.72$ for the TOC

(28) Santato, C.; Odziemkowski, M.; Ulmann, M.; Augustynski, J. *J. Am. Chem. Soc.* **2001**, *123*, 10639.
(29) Zhang, H.; Feng, M.; Liu, F.; Liu, L. B.; Chen, H. Y.; Gao, H. J.; Li. J. Q. *Chem. Phys. Lett*. **2004**, *389*, 337.
(30) Dresselhaus, M. S.; Dresselhaus, G.; Pimenta, M. A.; Eklund, P. C. In *Analytical Application of Raman Spectroscopy*; Pelletier, M. J., Ed.; Blackwell Science: Oxford, U.K., 1999; Chapter 9.

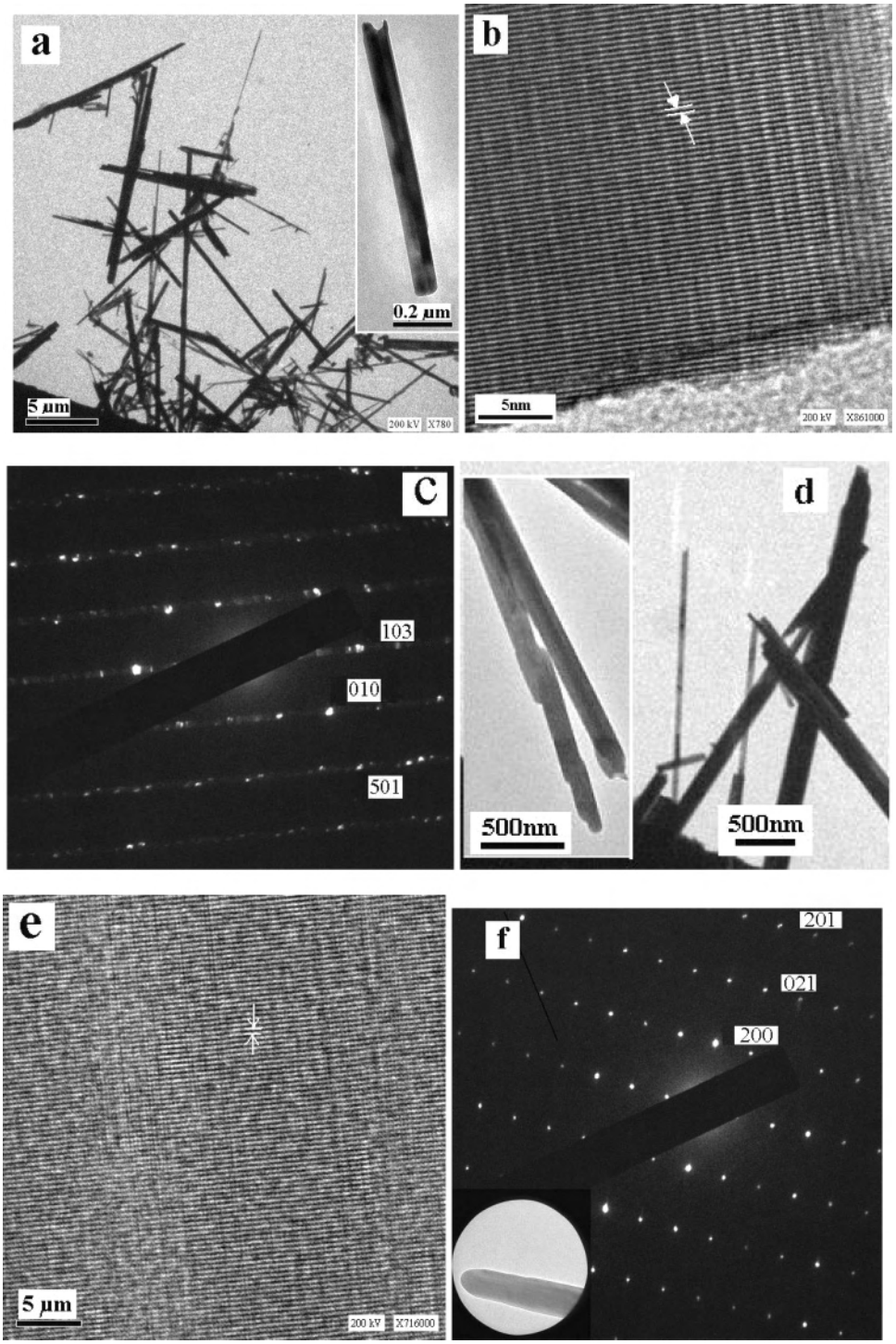

Figure 3. TEM images of (a) a TOC composite sample (inset: an individual nanorod), (b) an HRTEM image of an individual $W_{18}O_{49}$ nanorod, (c) an ED pattern of a $W_{18}O_{49}$ nanorod (respective planes are highlighted), (d) a TONR sample (inset: stacking of two nanorods), (e) an HRTEM image of an individual WO_3 nanorod, and (f) an ED pattern obtained from the WO_3 nanorod shown as an inset image.

product. It is suggested that the existence of the nongraphitic layers was a result of the relatively low reaction temperature of 700 °C, which is not high enough to permit an enhancement in the local order of the available carbon in the TOC composite.

The suggested mechanism was based on the obtained analytical data and on a few control experiments as well as on previously published data. From XRD, EDX, elemental (C, H, N, S) analysis, Raman spectroscopy, and HRTEM analysis, it was clear that the product, the TOC composite, was obtained as a result of the thermal dissociation of $WO(OMe)_4$ under an inert or air atmosphere. The composite was comprised of $W_{18}O_{49}$ nanorods with a small percent of carbon. A vapor−solid process was presumed to control the formation of the one-dimensional nanostructures, nanotubes, or nanowires.[10] According to our interpretation, all the products of the dissociation reaction floated in the gas phase and solidified right after their formation. We assumed that

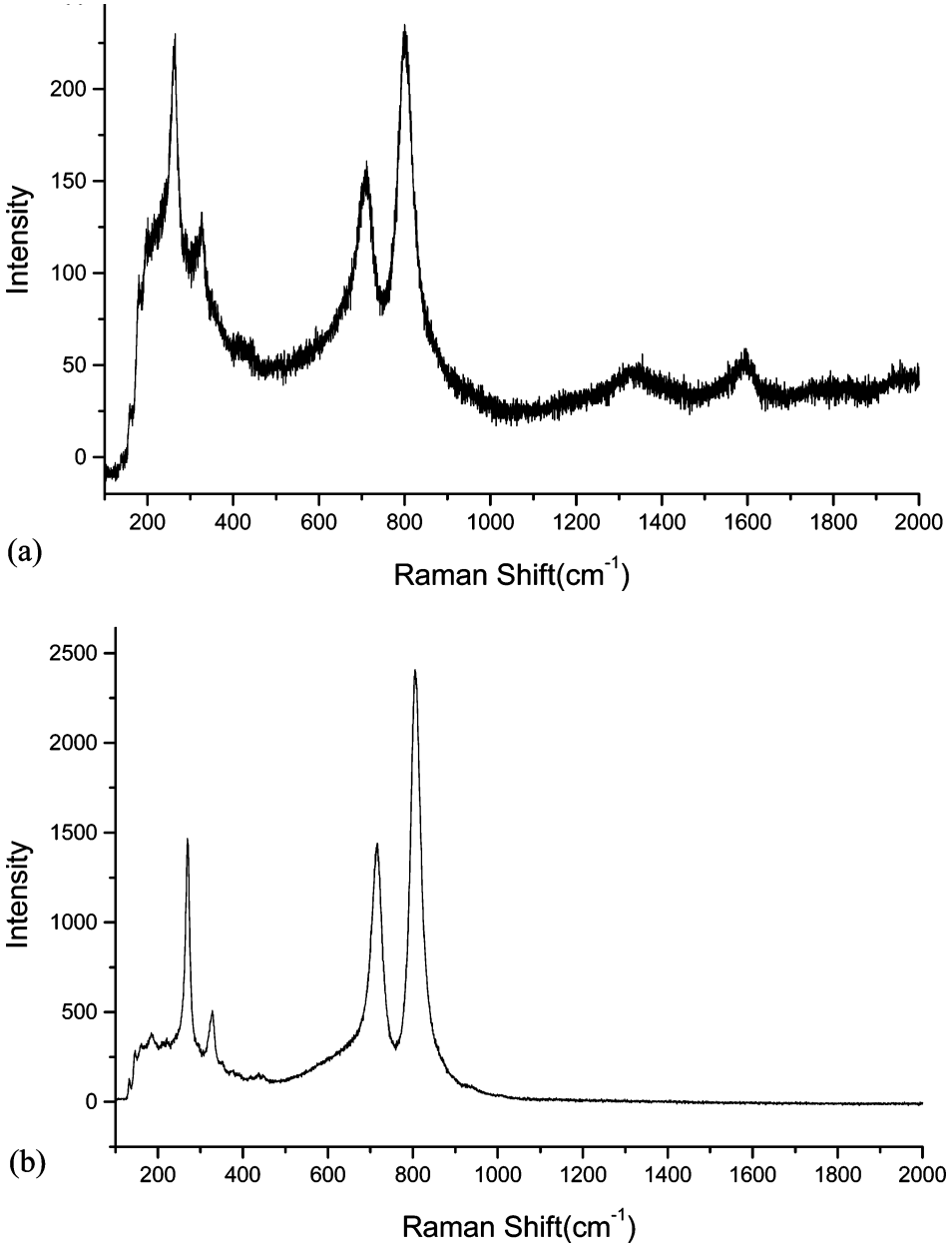

Figure 4. Micro-Raman spectra of (a) TOC and (b) WO_3 nanorods.

the dissociation of $WO(OMe)_4$ at 700 °C led to the immediate formation of WO_3 and C. Their self assembly in a rod shape was in accordance with a previous report that demonstrated that the direct heating of W filaments under air led to the formation of randomly distributed WO_3 nanorods on Si wafers.[31]

According to our interpretation, the presence of carbon after the 700 °C thermolysis implied that the carbon has partially reduced (five atoms of W^{6+}) the W^{6+} to W^{4+} and further acted as a nucleating center. The monoclinic $W_{18}O_{49}$ nanomaterial mostly possessed a layered[10] structure at a high temperature range. During cooling, the subsequent accumulation of several nuclei further oriented in a close-packed ⟨010⟩ plane under pressure resulted in the formation of $W_{18}O_{49}$ nanorods. It is also well-known that the substoichiometric WO_3 nanorods,[29] prepared at about 830 °C under an atmosphere of a H_2 and Ar mixture, could grow along either the ⟨001⟩ or the ⟨110⟩ planes with evident stacking faults and textural structure. For the intermediate oxides of tungsten, WO_x ($x = 2, 3$), when the value of x does not satisfy 3, the growth direction was limited by a planar defect of oxygen layers in the crystal, resulting in the spontaneous formation of a rod-shaped structure.[29]

Unlike in previous RAPETs of other transition metal (TM) alkoxides[17,19,22] where the core−shell of carbon and the TM oxide have often been formed, $W_{18}O_{49}$ and carbon were formed as separate entities and did not form core−shell structures. This was surprising because the controlled RAPET experiment of $W[OCH(CH_3)_2]_6$, 5% (w/v) in 2-propanol at 700 °C, yielded a core−shell structure where the carbon was the shell and the WO_x was the core (Figure 5a,b). The XRD pattern of the core−shell product is presented in Figure 6a.

(31) Li, Y. B.; Bando, Y.; Golberg, D.; Kurashima, K. *Chem. Phys. Lett.* **2003**, *367*, 214.

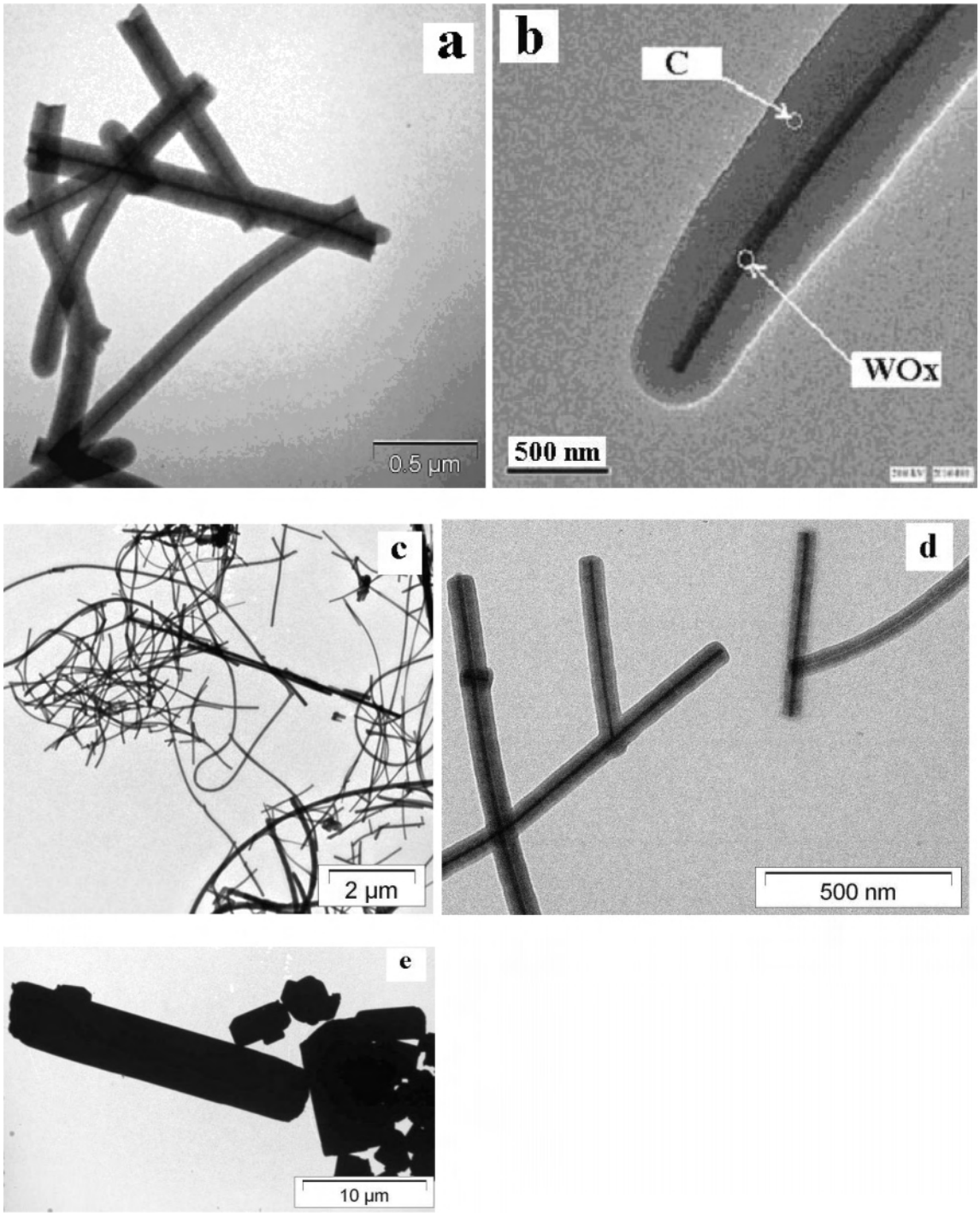

Figure 5. TEM image of tungsten(VI) isopropoxide, 5% (w/v) in 2-propanol dissociated at 700 °C yielded a core−shell structure where the carbon is the shell and the WO_x is the core. (a) Carbon sausages filled with tungsten oxide. (b) High-resolution image indicating the core and the shell, identified by SAEDX. (c) The wires produced after thermal decomposition of $WO(OMe)_4$ in ethanol at 700 °C. (d) The core−shell morphology of the wire shown with an HRTEM image. (e) The 20% (w/w) aqueous solution of $WO(OMe)_4$ was frozen to form ice, and then the formed precursor was used to carry out the RAPET at 700 °C for 3 h, which led to the formation of WO_3 microrods.

The major peaks appeared at 2θ values of 23.18, 23.48, 33.24, 40.77, 47.41, 53.61, and 59.03°, which correspond to the reflection lines of the monoclinic phase of the tungsten oxide (Table 1, expt no. 3). These values were in good agreement with the diffraction peaks, peak intensities, and cell parameters of crystalline $W_{24}O_{68}$. (PDF no. 36-103). When the RAPET of a 20 wt % solution of $WO(OMe)_4$ was carried out in ethanol instead of in 2-propanol, a similar morphology of the product was obtained (Figure 5c,d). Unlike the similar structure, the composition of the product from ethanol and the composition of the product from 2-propanol were different. The WO_x core was mainly composed of a mixture of WO_2 (PDF no. 32-1393) and $W_{18}O_{49}$ (PDF no. 1-84-1516), examined, and supported by the XRD measurements shown in Figure 6c (Table 1, expt no. 4). To further understand the origin of the reducing carbon, we have carried out the RAPET of a 20% (w/w) aqueous solution of $WO(OMe)_4$ at 700 °C for 3 h in ice.

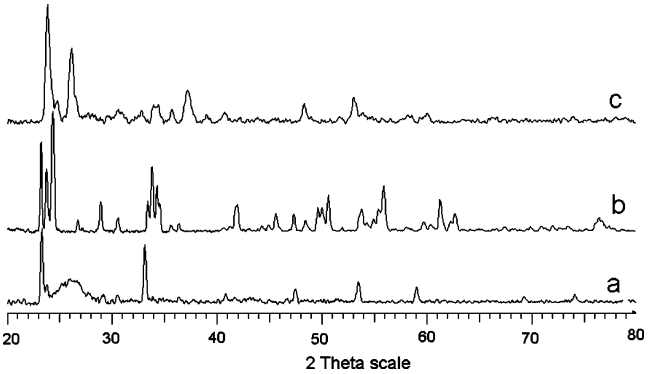

Figure 6. PXRD patterns of (a) thermally decomposed $WO(OMe)_4$ in 2-propanol at 700 °C, (b) thermally decomposed $WO(OMe)_4$ at 700 °C in ice, and (c) thermally decomposed $WO(OMe)_4$ in ethanol at 700 °C.

The resulting material was found to be a crystalline monoclinic phase of WO_3 (PDF no. 1-75-2072). However, in the current case, instead of forming core−shell structures, the formation of micrometer-size WO_3 rods took place (Table 1, expt no. 5). These rods had a diameter of around 2 μm and a length up to 10 μm (Figure 5e). The products were rod-shaped, but no reduction of the W^{6+} was detected.

It appeared that the core−shell structures were formed when a deep reduction of the metal cations could be achieved on the surface of nanoparticles. A very thin interface layer can be composed of a carbide or oxycarbide of the TM. The formation of the latter was clearly facilitated either by a strong tendency to reduce the metal cation [as always happens for Mo(VI), independent[27] of the nature of the alkyl group of the alkoxide ligand] or by the easy oxidation and polymerization of the alkoxide ligand through β-hydrogen atom transfer[25,26] (typical for the isopropoxide group). The absence of the formation of a core−shell structure can, thus, be explained in this case by an insufficiently deep reduction of the surface tungsten atoms by the methoxide ligands.

4. Conclusions

To summarize, we report a simple and efficient synthesis technique for the fabrication of WO_3 nanorods, without a catalyst, using a single precursor. The thermal dissociation of $WO(OMe)_4$ at 700 °C in a closed Swagelok cell under an air/inert atmosphere yielded a $W_{18}O_{49}$ nanorod, which was annealed at 500 °C under an air atmosphere to produce pure WO_3 nanorods. The mechanism of the formation of nonstoichiometric $W_{18}O_{49}$ nanorods with a nanometric diameter and a length of several micrometers was understood and proposed by carrying out several control experiments. The systematic characterization of the obtained materials was carried out by morphological (SEM and TEM), structural (XRD, HRTEM, and Raman spectroscopy), and compositional [EDX and elemental (C, H, N, S) analysis] measurements.

IC051179N